11th Australasian Fluid Mechanics Conference
University of Tasmania, Hobart, Australia
14-18 December 1992

TOPOLOGY AND TRANSPORT CHARACTERISTICS OF VORTICES IN A TURBULENT WAKE : EFFECT OF INITIAL CONDITIONS

Yu ZHOU and Robert A. ANTONIA

Department of Mechanical Engineering
University of Newcastle, NSW 2308, AUSTRALIA

ABSTRACT

A study has been made of turbulent vortices behind various wake-generating bodies with the same characteristic dimension h (circular, triangular and square cylinders and a screen of 50% solidity). Using orthogonal arrays of sixteen X-wires, eight in the (x, y) plane and eight in the (x, z) plane, velocity data have been obtained simultaneously in the two planes at $x/h = 20$ and Re ($\equiv U_0 d/\nu$) $= 5600$. The topology and transport characteristics of the vortices are sensitive to the initial conditions, in particular on whether the wake generating body is porous or impervious. The effect of initial conditions on the convection velocity of the vortices is also considered.

INTRODUCTION

The effect of the initial conditions on the behaviour of a plane wake has been investigated by a number of authors. Sreenivasan (1981) observed substantial differences in the manner wakes produced by different generators evolved, even though the shape of the mean velocity profile remained the same (when normalised by its own characteristic scales) in each case. Sreenivasan and Narasimha (1982) suggested that a unique self-preserving state existed for all plane wakes. Wygnanski et al. (1986) reported a dependence of the normalised distributions of the longitudinal turbulence intensity on the initial conditions. The more recent studies of Louchez et al. (1987), Cimbala et al. (1988) and Matsumura et al. (1991) have confirmed that the detailed behaviour of a turbulent wake (both near and far fields) is strongly dependent on the initial conditions. This, in effect, suggests that the characteristics of the vortical motion in the wake may differ as the initial conditions differ. This difference in vortical behaviour does not seem to have been well documented although matsumura et al. considered the spectral behaviour, topology and transport characteristics (i.e. contributions to the Reynolds stresses) of vortices in the near wakes of a screen (60% solidity)and a solid plate.

The main aim of the present study is to investigate the effect of different wake-generators on the topology and transport characteristics of turbulent vortices in the near field. We also consider the effect on the strength, convection velocity and two-dimensionality of the vortices.

EXPERIMENTAL DETAILS

Experiments were carried out in an open return low turbulence wind tunnel with a 2.4 m long working section (0.35 m × 0.35 m). The bottom wall was tilted to achieve a zero streamwise pressure gradient. Various wake-generators (circular, triangular and square cylinders and a screen of 50% solidity) of the same height ($h = 12.5$ mm) were used. Each generator was installed in the mid plane and spanned the full width of the working section, 20 cm from the exit plane of the contraction. This resulted in a blockage of about 3.6%. Measurements were made at $x/h = 20$ and a Reynolds number of 5600 (based on h and the free stream velocity U_0).

Orthogonal arrays of sixteen X-wires (see Figure 1 for spatial arrangement) were used for the simultaneous measurement of velocity fluctuations u, v in the (x, y) plane and u, w in the (x, z) plane ($y/h \simeq 0.7$). The possibility of interference of the X-wire arrays with the flow was checked and found to be negligible (Zhou and Antonia, 1992c). Wollaston (Pt-10% Rh) wires, 5 μm in diameter and about 1 mm in working length, were operated with constant temperature circuits. Signals from the circuits were offset, amplified and then digitised using two 16 channel (12 bit) A/D boards and two personal computers (NEC 386) at a sampling frequency of 3.5 kHz per channel. Data acquisition by the two computers was synchronised using a common external trigger pulse (the configuration is shown in Krogstad et al., 1992). Using velocity and yaw calibrations, signals proportional to u, v and w, together with the local mean velocities $\overline{U}, \overline{V}$ ($\simeq 0$) and $\overline{W}$ ($\simeq 0$), were formed on digital tape. The duration of each record was about 38 s. Subsequent data processing was done on a VAX 8550 computer.

VORTEX DETECTION

Vortices are identified — with respect to both time and lateral locations — by a method that includes criteria for vorticity concentration and circulation. Only a brief description is given here (for further details, see Zhou and Antonia, 1992a). Using instantaneous signals $U = \overline{U} + u$ and $V = \overline{V} + v = v$, an approximation to the instantaneous spanwise vorticity is

$$\omega_z \simeq \frac{\Delta V}{\Delta x} - \frac{\Delta U}{\Delta y} \quad ,$$

where $\Delta y \simeq 5$ mm is the spacing between X-wires and $\Delta x = -\Delta t\, U_{c0}$. U_{c0} ($= 0.87 U_0$) is the assumed convection velocity. The choice of U_{c0} is not critical for determining vortex locations (Zhou and Antonia, 1992b).

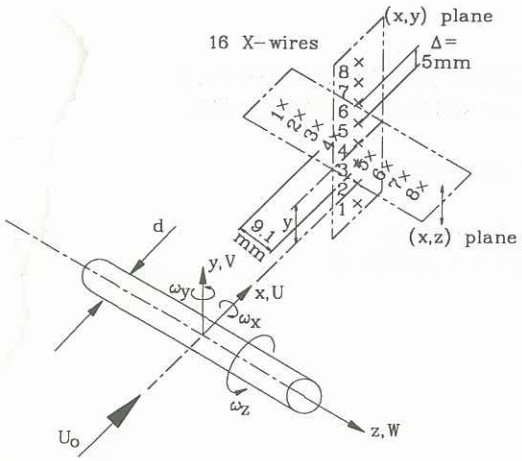

Figure 1 Experimental arrangement. (A circular cylinder is used for the purpose of illustration).

In the first criterion, the local peak values of ω_z, ω_{zp} say, are compared with the maximum mean shear $S_m = (\partial\overline{U}/\partial y)_{max}$. Specifically, a detection is first assumed to occur when

$$|\omega_{zp}| > k_\omega S_m \quad . \tag{1}$$

In (1), k_ω is a positive threshold, which is at first chosen arbitrarily and later modified after visually examining detection locations on instantaneous vorticity contour plots.

Before the second criterion is applied, the circulation Γ is calculated using the following equation

$$\Gamma = \int_0^{r_v} \left[\int_0^{2\pi} \omega_z(r,\theta) d\theta \right] r dr \quad , \tag{2}$$

where $\omega_z(r,\theta)$ is obtained by applying a surface-fit technique to vorticity data centred on ω_{zp} (i.e. the origin of the r,θ co-ordinate system is at the location of ω_{zp}). In Eq. (2), r_v is the vortex radius where the mean vorticity at a radius r from the vortex centre, defined by

$$\Omega_z(r) = \frac{1}{2\pi} \int_0^{2\pi} \omega_z(r,\theta) d\theta \tag{3}$$

drops to the assumed minimum vorticity level Ω_{zc} (> 0) for the vortex, viz.

$$|\Omega_z(r_v)| = \Omega_{zc} \quad . \tag{4}$$

Eq. (4) is solved for r_v by using a quasi-Newton optimising algorithm (Gill and Murray, 1976) which searches for the minimum of $[|\Omega_z(r)| - \Omega_{zc}]^2$. The magnitude of Γ determined from Eq. (2) is required to satisfy the following condition

$$|\Gamma| \geq k_\Gamma S_m h^2 \tag{5}$$

where k_Γ is a positive threshold determined in similar fashion to k_ω.

By varying k_ω and k_Γ, the number of detections is chosen to be about 2000 for the circular and triangular cylinders, 1400 for the square cylinder and 2800 for the screen. These numbers correspond to a detection frequency of half the vortex frequency f_0, which is identified by the location of the main peak in the v spectrum.

CONDITIONAL AND STRUCTURAL AVERAGES

The conditional average of an instantaneous quantity F is given by

$$<F>_k = \frac{1}{N} \sum_{m=1}^{N} F_{j_m+k}$$

where k represents time (in samples, positive or negative) relative to the detection points j_m and N is the total number of detections. (For convenience, the subscript k will be omitted). The conditional average of $\Omega_z(r)$ defined by Eq. (3) is specifically defined by

$$<\Omega_z>(r) = \frac{1}{N} \sum_{m=1}^{N} \Omega_{zm}(r) \quad .$$

F can be viewed as the sum of the time mean component $\overline{F}$ and the fluctuation component f. The latter can be further decomposed into the coherent fluctuation $\tilde{f} \equiv <f>$ and a remainder f_r, viz.

$$f = \tilde{f} + f_r \quad .$$

Also

$$<fg> = \tilde{f}\tilde{g} + <f_r g_r> \tag{6}$$

where f and g can each stand for either u or v.

If the conditionally averaged structure begins k_1 samples before the detection instant and ends k_2 samples after this instant, a structural average is denoted by a double overbar, e.g.

$$\overline{\overline{\tilde{f}\tilde{g}}} = \frac{1}{k_1 + k_2 + 1} \sum_{-k_1}^{k_2} \tilde{f}\tilde{g} \quad . \tag{7}$$

The value of k_1 ($= k_2$) is 15 for the circular and triangular cylinder wakes, 25 for the square cylinder wake and 11 for the porous-body wake so that the duration $(k_1 + k_2 + 1)$ corresponds to approximately the average time interval between structures in each flow.

RESULTS

A few properties of the detected vortices are summarised in Table I. The vortex frequency f_0 for the porous-body wake is largest corresponding to a Strouhal number of about 0.28. This number is about 0.2 for the circular and triangular cylinders and 0.12 for the square cylinder. This latter value is the same as that reported by Vickery (1966).

Wake Generator	$\frac{y_v}{h}$	$\frac{<U_c>}{U_0}$	$\frac{\lvert\omega_{zp}\rvert h}{U_0}$	$\frac{f_0 h}{U_0}$	$\phi_{uv}(f_0)$
Circular cyl.	0.5	0.87	1.63	0.21	$-94°$
Triang. cyl.	0.9	0.85	1.34	0.21	$-72°$
Square cyl.	0.7	0.85	2.05	0.12	$-112°$
Screen	0.7	0.78	0.95	0.28	$-169°$

Table I Some Characteristic Properties of Vortices

The convection velocity $<U_c>$ is given by the mean velocity at the vortex centres which are located on the most probable lateral position y_v, i.e. the vortex path. The value of y_v is estimated from a histogram (not shown here) of the lateral distribution of detections. In the porous-body wake, $<U_c>$ ($\simeq \overline{U}$) is noticeably smaller than in solid-body wakes. For a circular cylinder wake, Zhou and Antonia (1992a,b)

found that $<U_c>$ is greater than $\overline{U}$ and attributed this difference to the interaction between the opposite-signed vortices. This interaction, however, appears to be very weak in the porous-body wake, as indicated by the conditional sectional streamlines presented later in this section.

Another difference between vortices in porous- and solid-body wakes is the phase shift between u and v, given by $\phi_{uv}(f_0) \equiv \tan^{-1}[Q_{uv}(f_0)/C_{uv}(f_0)]$ where Q_{uv} is the quadrature spectrum and C_{uv} is the co-spectrum of u and v. The magnitude of $\phi_{uv}(f_0)$ is close to 90° for solid-body wakes but close to 180° for the porous-body wake. This implies that the coherent contribution to the Reynolds shear stress ($\overline{uv}$) may be small in solid-body wakes but significant in porous-body wakes. Results presented later in this section corroborate this implication.

Conditional sectional streamlines (Figure 2) suggest that the vortex shape, size and spacing may vary, especially between porous- and solid-body wakes. These differences may be related to the different vortex strengths among the different wakes. The largest vortex strength occurs for the square and circular cylinder wakes. Instantaneous streamlines suggest that for these flows, vortices tend to cross the centreline with higher frequency than in the porous-body wake, where the vortex strength is only about $50 \sim 60\%$ of that in the solid-body wakes. Note that vortices in the porous-body wake occur in a quasi-periodic fashion and alternate on either side of the centreline, as observed by Matsumura et al. (1991) [$Re = 11000$, $x/h = 24$].

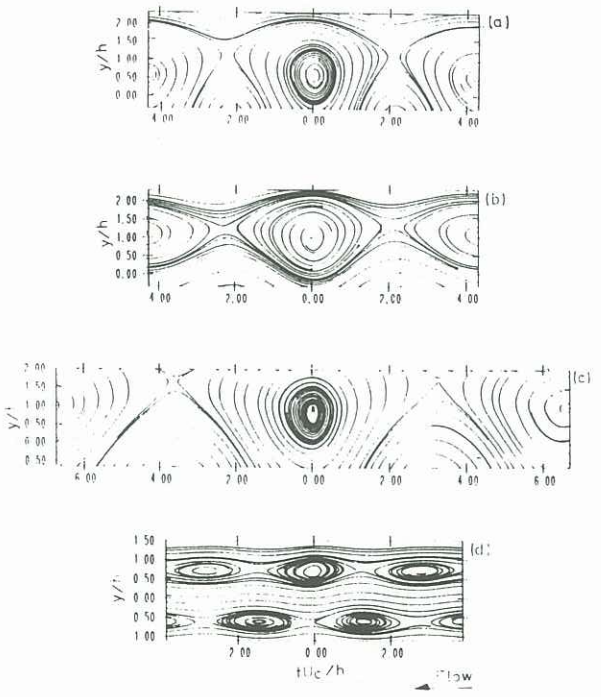

Figure 2 Conditional sectional streamlines. (a) circular cylinder; (b) triangular cylinder; (c) square cylinder; (d) screen.

The distributions of $\overline{u^2}$, $\overline{v^2}$, $\overline{uv}$ and $\overline{\tilde{u}^2}$, $\overline{\tilde{v}^2}$, $\overline{\tilde{u}\tilde{v}}$, in Figure 3 give some idea of the coherent contribution to the Reynolds stresses. It has already been noted that the lateral location of vortices may vary considerably, especially for solid-body wakes. Conditional quantities, particularly those associated with u, e.g. $\tilde{u}$ and $\tilde{u}\tilde{v}$, will therefore be

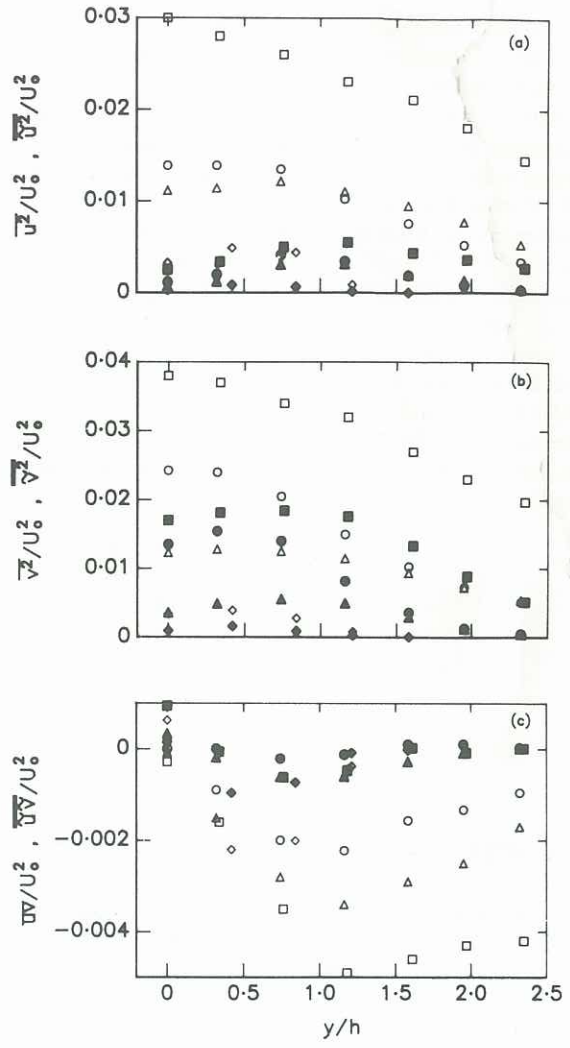

Figure 3 Conventional Reynolds stresses ($\overline{fg}/U_0^2$) [open symbols] and coherent contributions ($\overline{\tilde{f}\tilde{g}}/U_0^2$) [solid symbols]. (a) $f = g = u$; (b) $f = g = v$; (c) $f = u$; $g = v$. ○, circular cylinder; △, triangular; □, square; ◇, screen.

smeared or underestimated if vortices are aligned only with respect to time (thus ignoring the jitter in their y locations). To reduce this smearing, vortices have been separated into five subsets according to their lateral location and $\overline{\tilde{f}\tilde{g}}$ in Figure 3 is calculated from

$$\overline{\tilde{f}\tilde{g}} = \sum_{j=1}^{5} \frac{N_j}{N} (\overline{\tilde{f}\tilde{g}})_j \quad , \tag{8}$$

where $(\overline{\tilde{f}\tilde{g}})_j$ is the structural average of the j^{th} subset with N_j the number of detections for this subset. For all the structural averages presented here, it has been verified that $\overline{<fg>}$ is approximately equal to $\overline{fg}$ (the maximum departure is of order 10%), implying that the detections are reasonably representative of the flow. Figure 3 indicates that the maximum values of $\overline{\tilde{v}^2}$ and $\overline{\tilde{u}\tilde{v}}$ tend to occur approximately along the vortex path ($y/h \simeq 0.5 \sim 0.7$), while the maximum value of $\overline{\tilde{u}^2}$ occurs slightly above the vortex path ($y/h \simeq 0.7 \sim 1.2$). The maximum (percentage) values of $\overline{\tilde{f}\tilde{g}}/\overline{fg}$ are shown in Table II. The coherent contribution to $\overline{v^2}$ is almost twice that to $\overline{u^2}$. This may be related to

the considerably larger uncertainty of vortex location in the lateral direction (= ± 0.5 X-wire spacing $\simeq \pm 2.5$ mm) than in the longitudinal direction (= $\pm 0.5 U_c$/sampling frequency $\simeq \pm 0.8$ mm for solid-body wakes). This large uncertainty will inevitably result in $\tilde{u}$ and hence $\overline{\overline{\tilde{u}^2}}$ and $\overline{\overline{\tilde{u}\tilde{v}}}$ being underestimated, despite the use of Eq. (8). Table II indicates that the coherent contribution to $\overline{u^2}$ and $\overline{v^2}$ is higher in solid-body wakes ($30 \sim 70\%$) than in the porous-body wake ($20 \sim 40\%$). The contribution to $\overline{uv}$ is however smaller for solid-body wakes ($5 \sim 20\%$) than for the porous-body wake ($\simeq 40\%$). The different contributions to $\overline{uv}$ is consistent with the observed phase shift between u and v within vortices. For solid-body wakes, $\phi_{uv}(f_0)$ is close to 90° (Table I) and the average product of u and v tends to be minimised; for the porous-body wake, however, $\phi_{uv}(f_0)$ is close to 180° and the magnitude of this product tends to be maximised.

Wake Generator	$\frac{\overline{\overline{\tilde{u}^2}}}{\overline{u^2}}$	$\frac{\overline{\overline{\tilde{v}^2}}}{\overline{v^2}}$	$\frac{\overline{\overline{\tilde{u}\tilde{v}}}}{\overline{uv}}$
Circular cylinder	34	68	4
Triangular cylinder	28	44	21
Square cylinder	28	55	18
Screen	18	41	44

Table II Maximum Coherent Contributions (%) to Reynolds Stresses

CONCLUSIONS

The behaviour of vortices in wakes from two-dimensional bodies depends on the initial conditions. The difference between porous- and solid-body wakes is particularly noticeable with respect to the convection velocity, topology and transport properties of the vortices. Vortices in solid-body wakes contribute more to $\overline{u^2}$ and $\overline{v^2}$ but considerably less to $\overline{uv}$ than those in the porous-body wake.

ACKNOWLEDGEMENT

The authors acknowledge Mr. J. Mi's contribution to experiments. The support of the Australian Research Council is gratefully acknowledged.

REFERENCES

CIMBALA, J. M., NAGIB, H. M. and ROSHKO, A. (1988) Large Structure in the Far Wakes of Two-Dimensional Bluff Bodies, *J. Fluid Mech.*, **190**, 265.

GILL, P. E. and MURRAY, W. (1976) Minimization Subject to bounds on the Variations, *Report NAC 72*, National Physical Laboratory.

KROGSTAD, P-Å., ANTONIA, R. A. and BROWNE, L. W. B. (1992) Structure Investigation in a Turbulent Boundary Layer Using Orthogonal X-Wire Arrays, *11th Australasian Fluid Mechanics Conference*, (to be presented).

LOUCHEZ, P. R., KAWALL, J. G. and KEFFER, J.F. (1987) Detailed Spread on Characteristics of Plane Turbulent Wakes, *Proc. 5th Symposium on Turbulent Shear Flows*, Lecture Notes in Physics, Springer, 98-109.

MATSUMURA, M., HUANG, Z., KAWALL, J. G. and KEFFER, J. F. (1991) Coherent Structures in the Turbulent Wake of a Porous Body, *Proc. Eighth Symposium on Turbulent Shear Flows*, Munich, 28-2.

SREENIVASAN, K. R. (1981) Approach to Self-Preservation in Plane Turbulent Wakes, *AIAA Jnl.*, **19**, 1365.

SREENIVASAN, K. R. and NARASIMHA, R. (1982) Equilibrium Parameters for Two Dimensional Turbulent Wakes, *J. Fluids Eng.*, **104**, 167.

VICKERY, B. J. (1966) Fluctuating Lift and Drag on a Long cylinder of Square Cross-Section in a Smooth and Turbulent Stream, *J. Fluid Mech.*, **25**, 481-494.

WYGNANSKI, I., CHAMPAGNE, F. and MARASLI, B. (1986) On the Large-Scale Structures in Two-Dimensional, Small-Deficit, Turbulent Wakes, *J.Fluid Mech.*, **168**, 31-71.

ZHOU, Y. and ANTONIA, R. A. (1992a) A Study of Turbulent Vortices in the Near-Wake of a Cylinder, *J. Fluid Mech.*, (submitted).

ZHOU, Y. and ANTONIA, R. A. (1992b) Convection Velocity Measurements in a Cylinder Wake, *Expts. in Fluids*, **13**, 63-70.

ZHOU, Y. and ANTONIA, R. A. (1992c) A Study of Flow Properties Near Critical Points, *IUTAM Symp. "Eddy Structure Identification in Free Turbulent Shear Flows"*, Poitiers (to be presented).